# Nonresonant multiphoton ionization of calcium atoms in an intense laser field

L. F. DiMauro
*Department of Chemistry, Brookhaven National Laboratories and Associated Universities, Upton, New York 11973*

Dalwoo Kim, M. W. Courtney, and M. Anselment
*Department of Physics, Louisiana State University, Baton Rouge, Louisiana 70803*
(Received 13 April 1988)

We have studied the single and double nonresonant multiphoton ionization of calcium atoms using both 532-nm and 1.06-$\mu$m radiation. These studies were conducted in the intensity regime of $10^{10}$–$10^{13}$ W/cm$^2$. We use mass and angularly resolved electron-energy analysis in an attempt to gain insight into the dominant mechanisms responsible for ionization. An analysis is presented for intensity- and frequency-dependent results, and electron angular distributions are reduced in terms of atomic parameters derivable from lowest-order perturbation theory.

## I. INTRODUCTION

In recent years there has been a considerable amount of interest in the behavior of atoms in intense laser fields. One of the critical questions raised by these studies is how much does our view of electric dipole transitions alter in the nonperturbative regime of the electromagnetic field. Experiments have revealed a number of new and dramatic effects, including above-threshold ionization[1–4] (ATI), multiple-charge-state distributions[5–7], short-wavelength generation,[4] and strong-field ionization.[8] Many theoretical models[9–15] have been proposed to describe the salient features of these observations. Although each has led to a further understanding of these effects, a great deal of controversy still remains. One example is the mechanism responsible for the observation of the relatively large abundance of highly charged states in the nonresonant multiphoton ionization (MPI) of atoms. One model[11] suggests that a collective or direct ionization process is occurring at these intensities, while Lambropoulos and co-workers[9,10] have proposed a model that describes these results in terms of sequential ionization and the temporal dynamics governing a particular experiment. The fundamental difference is that in the first case the process is viewed as the simultaneous ejection of many electrons, whereas with the second case it is described by sequential removal of single electrons.

Although the extent to which multiple-electron excitation is responsible for the production of multiple-charge-state distributions in closed-shell atoms is still unclear, a number of recent studies[16–18] have focused on determining the role of doubly excited states in the MPI of alkaline-earth atoms. The alkaline-earth atoms are attractive systems for MPI studies for a number of reasons. First, they contain a manifold of doubly excited states just above the first ionization threshold and in some cases even have bound doubly excited states. Second, they offer the opportunity to examine these effects at moderate laser intensities, where $I < 10^{13}$ W/cm$^2$. Finally, the low-$Z$ alkaline-earth atoms such as calcium and magnesium are systems that should prove to be theoretically tractable. This is especially relevant considering the recent success of Kim and Greene[19,20] on the single-photon ionization of calcium atoms.

In this paper we report the results of a nonresonant multiphoton ionization study on calcium atoms with 1.06- and 0.532-$\mu$m radiation in the regime of $I < 10^{13}$ W/cm$^2$. We use mass analysis and angularly resolved electron-energy analysis in an attempt to gain insight into the dominant mechanisms responsible for ionization. An analysis is presented for intensity- and frequency-dependent results and electron angular distributions are reduced in terms of atomic parameters derivable from lowest-order perturbation theory.[21,22] The main conclusions based on our own analysis and comparisons to other studies are as follows.

(1) Electron correlations play a significant role in the nonresonant multiphoton excitation of calcium atoms for both 1.06- and 0.532-$\mu$m radiation. Consequently an independent-electron description of the above processes will prove to be only approximate.

(2) The dominant process responsible for the production of doubly ionized calcium, $Ca^{2+}$, proceeds via sequential ionization. However, our results suggest that appropriate choice of experimental parameters could result in direct ionization.

A description of the experimental apparatus is given in Sec. II. Section III is devoted to a general discussion of the relevant features needed for interpreting the subsequent observations, especially as they pertain to calcium. Section IV is a detailed presentation and analysis of the experimental results including electron energy analysis, intensity effects, and electron angular distributions. The conclusion summarizes the findings of this study and identifies areas of future investigation.

 

## II. EXPERIMENTAL

A block diagram of the experimental apparatus is illustrated in Fig. 1. An amplified Nd:YAG (yttrium aluminum garnet) laser is used in the experiments operating in a near-Gaussian transverse mode and produces 1.5 J of 1.06-$\mu$m light in a 10-nsec pulse. Careful steps are taken to monitor and control the laser parameters. For all measurements the laser operates at fixed energy output, and any attenuation of the energy is accomplished by external optics consisting of a half-wave plate followed by a Brewster angle polarizer. Rotation of the laser polarization with respect to the detector is accomplished with a half-wave plate. The retardation plates are aligned using independent checks to minimize any asymmetries caused by imperfect optics. The light is focused into the interaction region by a 100-mm or a 250-mm focal length lens. The focus of both lenses for the YAG fundamental (1.06-$\mu$m) and second harmonic (532-nm) wavelengths are carefully measured using imaging techniques. Our absolute intensity is known with an accuracy of 30%. The laser energy is constantly monitored during a data run and the shot-to-shot fluctuations are kept to $\pm 1\%$.

The vacuum system is a differentially pumped atomic-beam apparatus. The calcium source chamber has an effusive oven and is evacuated by a liquid-$N_2$-trapped 6-in. diffusion pump. A 1-mm skimmer separates the source from the interaction-region chamber. The interaction region is surrounded by a 3-in. cylindrical conetic magnetic shield which also provides shielding for the drift region of the electron spectrometer. The laser and atomic beams intersect at right angles in the shielded region via four axial holes in the shield. Located outside the shielded region is a similar 6-in. diffusion pump system to handle the load of the atomic beam. This region of the chamber is maintained at $10^{-8}$ Torr. In order to reduce the pressure in the interaction region a 360 l/sec turbomolecular pump independently evacuates the inner volume of the cylindrical shield. This method achieves a pressure in the interaction region of $10^{-9}$ Torr. This is especially crucial since all the experiments are performed using low atomic-beam densities in order to minimize any effects caused by space charge.

The time-of-flight (TOF) spectrometer consists of a 2.5-cm diameter, 30-cm-long, magnetically shielded copper Faraday cage. A thin molybdenum circular plate with a 5-mm-diam hole bored at its center is placed at the beginning of the flight tube and acts as the entrance aperture of the spectrometer. This plate provides both a defining aperture for the spectrometer which minimizes stray background counts and a means of providing further differential pumping of the TOF spectrometer with a 55 l/sec turbomolecular pump. The spectrometer is maintained at a pressure of $10^{-9}$ Torr during a data run. A dual microchannel plate (MCP) detector at the end of the drift tube provides an angular resolution of $2\times 10^{-3}$ sr with respect to the source. The signal from an impedance-matched 50-$\Omega$ conical anode is fed to a 200-MHz discriminator. Care is taken to ensure that no pulse pileup occurs and that the statistics are representative of single-electron counts. The discriminated output is then fed into a 200-MHz transient recorder. The overall reso-

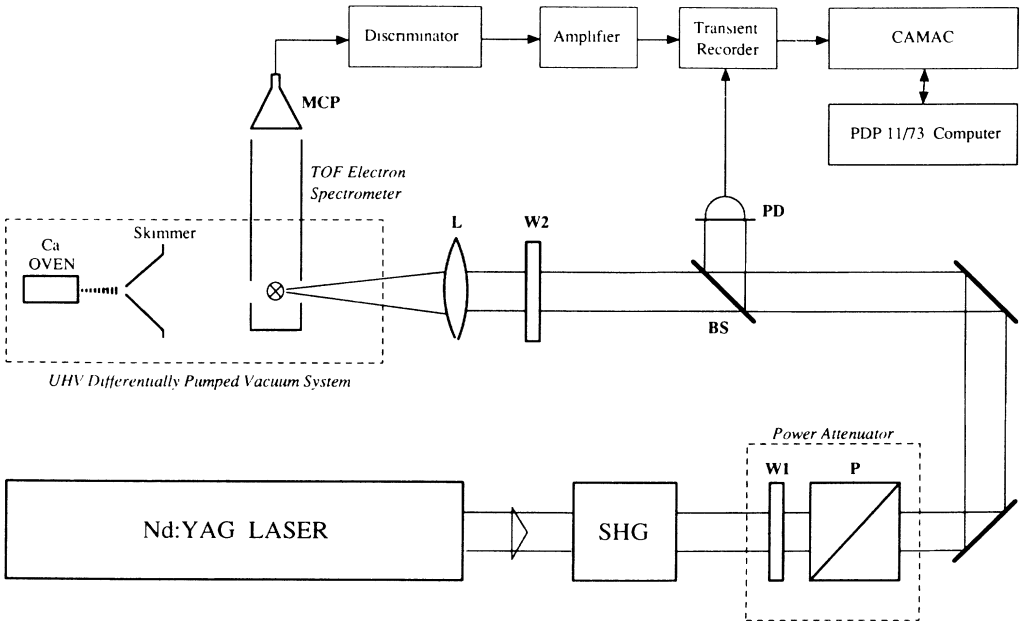


FIG. 1. Block diagram of the apparatus, described in text. The power attenuator consists of a half-wave plate, W1, and polarizer, P. The harmonic generator, SHG, is used only in the 532-nm studies. The polarization of the laser is rotated by means of a half-wave plate, W2. A beam splitter, BS, reflects part of the laser beam to a photodiode, PD. The analog signal from PD is used to trigger the transient recorder and provide a constant monitor of the laser energy. The laser and atomic beams intersect at right angles and are only shown in the figure as collinear for illustrative convenience.

lution of the spectrometer is approximately 60 meV at an energy of 1 eV. The electron spectrometer is calibrated by recording and analysis of the MPI spectrum of xenon. The transient recorder is interfaced to a PDP 11/73 computer via a CAMAC acquisition system. The electron spectrum is recorded for every laser shot and the maximum number of total ion yield per laser shot is limited to 50–100 ions. This reduces to approximately one electron count per shot detected through the spectrometer's acceptance angle when the laser's polarization is parallel to the detector's axis.

## III. GENERAL CONSIDERATIONS

A brief presentation of the processes and concepts relevant to our discussion of the experimental results is warranted. The ionization threshold values from the ground state of the neutral and singly ionized calcium are 6.11 and 11.87 eV, respectively, as illustrated in Fig. 2. The lowest-order ionization process for neutral ground-state calcium with 532-nm radiation is

$$\mathrm{Ca}(4s^2)+3h\nu\rightarrow\mathrm{Ca}^+(4s)+e(0.88\ \mathrm{eV})\ . \quad (1)$$

Similarly for 1.06-$\mu$m radiation,

$$\mathrm{Ca}(4s^2)+6h\nu\rightarrow\mathrm{Ca}^+(4s)+e(0.88\ \mathrm{eV})\ . \quad (2)$$

The kinetic energy of the ejected electron is given in the parentheses and the equation number correlates with the paths illustrated in Fig. 2. Sequential ionization results in the creation of doubly ionized calcium by subsequent excitation of the ground-state ions created in the first two paths. For lowest-order ionization with 532-nm radiation,

$$\mathrm{Ca}^+(4s)+6h\nu\rightarrow\mathrm{Ca}^{2+}(3p^6)+e(2.11\ \mathrm{eV})\ ; \quad (3)$$

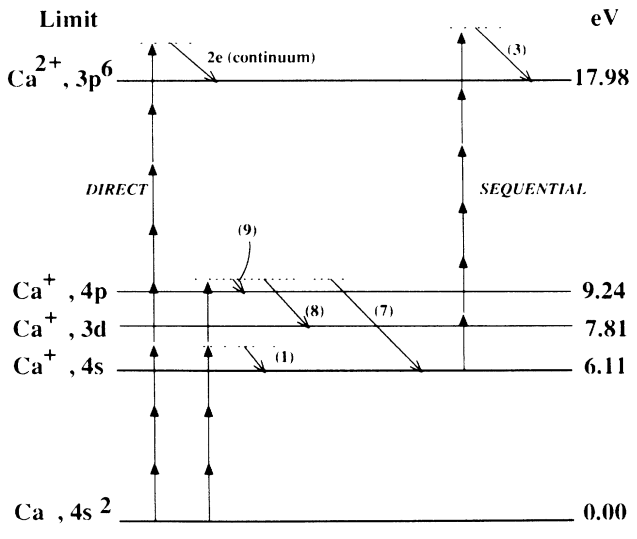


FIG. 2. Energy-level diagram for calcium showing threshold levels relevant to this study. The numbers in parenthesis correlate with the equations given in the text. The energies for the threshold levels are referenced with respect to the neutral calcium $4s^2$ ground state.

while for 1.06-$\mu$m excitation,

$$\mathrm{Ca}^+(4s)+11h\nu\rightarrow\mathrm{Ca}^{2+}(3p^6)+e(0.95\ \mathrm{eV})\ . \quad (4)$$

All of the above multiphoton processes are adequately described by (a) a model incorporating the transition dynamics for single-electron ionization, that is, each process results in a free electron and a ground-state ion and (b) the dynamics of the laser pulse.

A sharp deviation from this simple single-electron picture is direct double ionization of neutral calcium above the two-electron escape limit. The result of this will be the simultaneous ejection of two "correlated" electrons. An 8-photon absorption of 532-nm radiation yields

$$\mathrm{Ca}(4s^2)+8h\nu\rightarrow\mathrm{Ca}^{2+}(3p^6)+2e(\mathrm{continuous})\ ; \quad (5)$$

while 1.06-$\mu$m photon absorption proceeds via

$$\mathrm{Ca}(4s^2)+16h\nu\rightarrow\mathrm{Ca}^{2+}(3p^6)+2e(\mathrm{continuous})\ . \quad (6)$$

The signature for this process will be distinctive from paths (1) through (4). First and most obvious, the order of nonlinearity is higher for paths (5) and (6) than for any of the individual sequential processes. Second, instead of discrete electron peaks, one would expect to observe a flat continuous spectrum from zero energy up to the maximum kinetic energy. This maximum kinetic energy is determined by the excess energy of the $N$th photon absorption above the two-electron threshold. The simple physical interpretation is that all combinations for sharing the excess energy between the two electrons are equally probable. Furthermore, a closer theoretical[23] examination for single-photon absorption reveals a slight preference or cusp in the distribution at half the maximum kinetic energy. A number of groups[17,18,24] have looked for explicit evidence for direct ionization with no satisfactory results. Although the spectral and angular earmark for this process is quite distinct from sequential ionization, practical experimental difficulties at these intensities render detection of direct ionization difficult, i.e., contributions from background electrons.

Above-threshold ionization has been studied extensively in the rare gases by various groups[1–3,25] and the results are satisfactorily described in terms of the one-electron model. This is partially due to the fact that in the rare gases no multiply excited states exist close to threshold. However, for calcium, as well as other alkaline-earth atoms, additional photon absorption can result in a physical picture quite different from "single-electron" ATI. This is a consequence of the atomic structure of calcium where doubly-excited-state manifolds are found close to threshold and represent additional open decay channels. This is seen in Fig. 2, where the $3d$ and $4p$ thresholds lie approximately 1.6 and 3.1 eV above the $4s$ limit. In addition, some of the doubly excited states are bound in the neutral, i.e., $4p^2$, $3d^2$ states. Consequently, there is an enhanced probability that the multiphoton process will acquire some double-excitation character and possibly lead to an observable branching ratio for direct two-electron ionization. Specifically, if an additional fourth 532-nm photon is absorbed in the continuum the excitation results in three open decay channels:

$$\mathrm{Ca}(4s^2)+(3+1)h\nu \begin{cases} \rightarrow \mathrm{Ca}^+(4s)+e(3.21\ \mathrm{eV})\ \ \mathrm{ATI} & (7) \\ \rightarrow \mathrm{Ca}^+(3d)+e(1.51\ \mathrm{eV}) & (8) \\ \rightarrow \mathrm{Ca}^+(4p)+e(0.07\ \mathrm{eV})\ . & (9) \end{cases}$$

Path (7) is an electron decay channel which results in a spectrum similar to that observed in the ATI of rare-gas atoms. The kinetic energy of the electron in path (7) differs from the electron energy in path (1) by the photon energy. However, paths (8) and (9) leave the ion in an excited $3d$ metastable state and excited $4p$ state, respectively. The salient point is that the final state of the process results in two excited electrons and consequently the single-electron model breaks down. Likewise, paths (1) and (7) would have also evolved with some probability of two-electron correlation. Thus, we see a clear distinction could exist between the mechanisms responsible for ATI in rare gases and alkaline-earth atoms. In a similar manner, for 1.06-$\mu$m excitation the absorption of one and two additional photons results in

$$\mathrm{Ca}(4s^2)+(6+1)h\nu \begin{cases} \rightarrow \mathrm{Ca}^+(4s)+e(2.04\ \mathrm{eV})\ \ \mathrm{ATI} & (10) \\ \rightarrow \mathrm{Ca}^+(3d)+e(0.35\ \mathrm{eV}) & (11) \end{cases}$$

and

$$\mathrm{Ca}(4s^2)+(6+2)h\nu \begin{cases} \rightarrow \mathrm{Ca}^+(4s)+e(3.21\ \mathrm{eV})\ \ \mathrm{ATI} & (12) \\ \rightarrow \mathrm{Ca}^+(3d)+e(1.51\ \mathrm{eV}) & (13) \\ \rightarrow \mathrm{Ca}^+(4p)+e(0.07\ \mathrm{eV})\ . & (14) \end{cases}$$

The (6+1) process leads to two open decay channels, $4s$ and $3d$, and the (6+2) process leads to the addition of the $4p$ decay channel. There are many other higher-order processes that could be included in this discussion, e.g., ionization of $Ca^+$ from an excited initial state. We limit this discussion only to those processes that are currently observable with our detection sensitivity but do not exclude the others as relevant mechanisms.

## IV. RESULTS AND DISCUSSION

### A. Energy spectrum

The electron energy spectrum of calcium with 532-nm excitation at an intensity of $1.7\times10^{12}$ W/cm$^2$ is shown in Fig. 3. The laser polarization direction is along the axis of detection. Clearly, the most dominant peak in the electron spectrum is the three-photon ionization of the $4s^2$ ground state of calcium via path (1). Also evident is a peak at an electron energy of 2.11 eV which can be unambiguously assigned to the 6-photon ionization of the $Ca^+$ ion via path (3). The mass spectrum shown in Fig. 4 verifies the presence of both singly and doubly ionized calcium at this intensity. Consequently, the results demonstrate that sequential ionization is the predominant mechanism for the production of the observed ion distributions in calcium. This result is consistent with observations made in other alkaline-earth atoms.[17,18] However, this conclusion does not presume that the transition dynamics are restricted to an independent-electron description. Referring to Fig. 3(b), we also observe peaks corresponding to the absorption of additional photons producing electrons with energies of 3.21 eV ($h\nu$+0.88 eV) via path (7) and 4.44 eV ($h\nu$+2.11 eV) for the $Ca^{2+}(3p^6)$ final state. Moreover, the absorption of additional photons also opens new electron decay channels. Closer examination of the electron spectrum in Fig. 3(b) reveals the presence of a peak at 1.51 eV which is attributable to the $Ca^+$ ion being left in the $3d$ excited state via path (8). Consequently, the multiphoton ionization of calcium proceeds with some probability for two electron or double excitation. Furthermore, electron peaks at 0.07 and 2.40 eV ($h\nu$+0.07 eV) are tentatively assigned to the (3+1) photon ionization via path (9) and the (3+2) ionization, respectively. Each of them results in a $Ca^+$ ion being left in a $4p$ excited state. Our inability to reproduce reliably the relative intensity of the 0.07-eV peak makes this assignment somewhat tentative. We believe that the source of this problem lies in the transmission characteristics of our spectrometer for electrons with energies below 100 meV. However, the observation of the second electron peak in the series with an energy of 2.4 eV ($h\nu$+0.07 eV) lends some credence to this assignment. It is worth remembering that the measured relative intensities of the peaks are not necessarily representative of the electron-decay branching ratios since our spectrometer

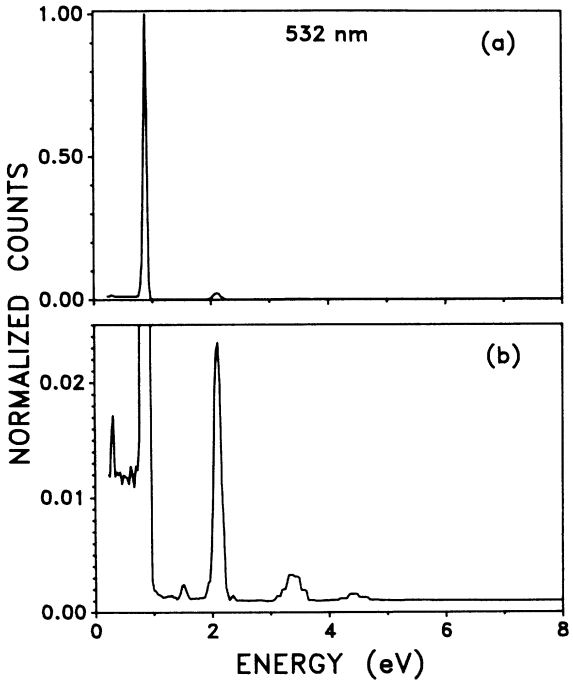


FIG. 3. Electron spectrum of calcium resulting from 532-nm excitation. The intensity is $1.7\times10^{12}$ W/cm$^2$ and the light is polarized along the detector axis. (b) is expanded by a factor of 40 in the $y$ axis.

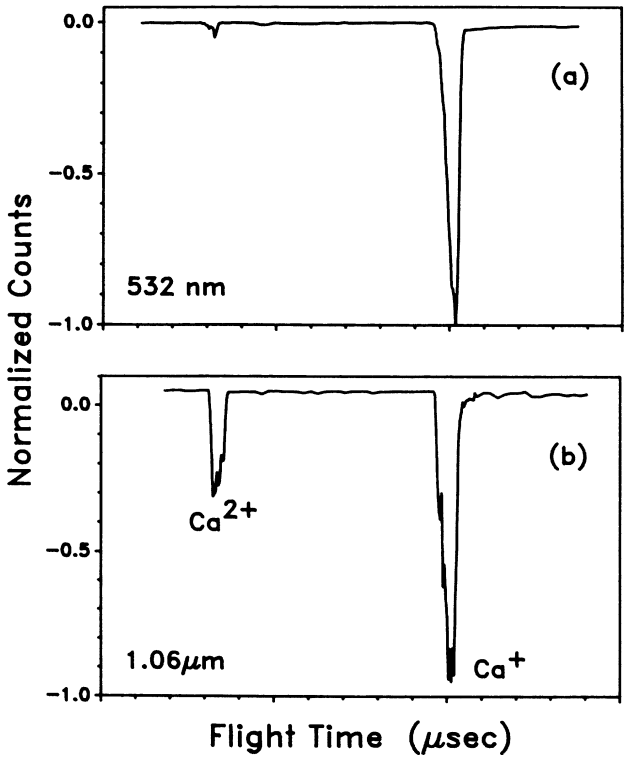


FIG. 4. Time-of-flight mass spectrum of calcium resulting from (a) 532-nm and (b) 1.06-$\mu$m radiation. The intensities for (a) and (b) are $7.0\times10^{11}$ W/cm$^2$ and $7.5\times10^{11}$ W/cm$^2$, respectively.

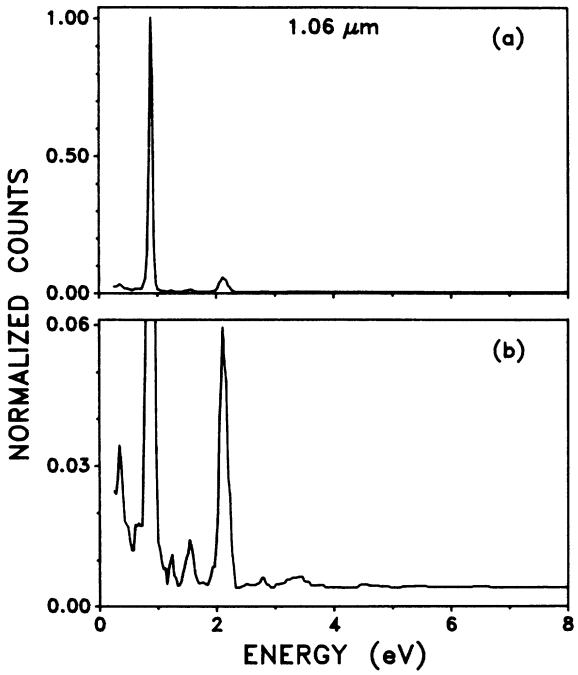


FIG. 5. Electron spectrum of calcium resulting from 1.06-$\mu$m excitation. The intensity is $3.4\times10^{12}$ W/cm$^2$ and the light is polarized along the detector axis. (b) is expanded by a factor of 16 in the $y$ axis.

views only a small solid angle. This is especially true for the double excitation channels where the angular anisotropy could be quite complex. Future plans include the addition of a $2\pi$ electron spectrometer to increase the electron transmission and provide more precise branching ratios.

Figure 5 shows an electron-energy spectrum of calcium resulting from excitation with 1.06-$\mu$m photons at an intensity of $3.4\times10^{12}$ W/cm$^2$. A number of higher-order peaks are observed in this spectrum but again the dominant peak has an energy of 0.88 eV. This peak is observed to be the major feature at all intensities. Unfortunately, at intensities exceeding $10^{11}$ W/cm$^2$, a problem exists at this wavelength in the absolute interpretation of this peak and its subsequent ATI peaks. This problem is a consequence of the near degeneracy of the electron energies for calcium for paths (2) and (4). Each process results in electrons with kinetic energies of 0.88 and 0.95 eV, respectively, which are unresolvable with our spectrometer. Obviously the same ambiguity persists for the ATI peaks with electron energies at 2.04 eV ($h\nu+0.88$ eV), 3.21eV($2h\nu+0.88$ eV), and 4.36 eV ($3h\nu+0.88$ eV). However, at low intensities, $I<10^{11}$ W/cm$^2$, the spectrum is seen to consist of a strong peak at 0.88 eV which is unambiguously assignable to path (2) and its associated ATI peak at 2.04 eV via path (10). At these low intensities the mass spectrum verifies that only singly ionized calcium is present. But as the intensity is raised above $10^{11}$ W/cm$^2$ the mass spectrum shows that the formation of $Ca^{2+}$ is significant. Likewise, the peaks in the electron spectrum at 0.88 and 2.04 eV broaden and are probably showing the effects due to contributions from the path (4) series. Also, at these intensities the higher ATI peaks at 3.34 eV ($S=2$) and 4.44 eV ($S=3$) start becoming evident. Here $S$ represents the number of additional photons absorbed in the continuum. Presumably these higher-order processes are a major consequence of path (4) and not of path (2). This would be consistent with higher-order ATI peaks being observed in higher-order ionization processes.

Again the main focus of attention in Fig. 5(b) is the electron peaks at energies of 0.35, 1.23, 1.51, and 2.68 eV. The assignment of all these peaks characterizes the final state of the ion as excited, that is either a $3d$ or a $4p$ state. The $3d$ series is $Ca(4s^2)+(6+S)h\nu\rightarrow Ca^{+}(4p)+e$, where the electron energies at 0.35, 1.51, and 2.68 eV correspond to $S=1$, 2, and 3, respectively. Likewise, the peak at 1.23 eV corresponds to the ion being left in the $4p$ state following a (6+3) photon absorption with $S=3$. The lowest energy electron from path (14) at 0.07 eV is difficult to observe in the electron spectrum at 1.06 $\mu$m. The difficulty in detecting this peak may be twofold. First, the transmission problems associated with our spectrometer, as discussed above. Second, with 1.06-$\mu$m radiation and intensities exceeding $10^{11}$ W/cm$^2$ suppression of the lowest energy peak by the ponderomotive potential may become significant. An intensity of $3\times10^{11}$ W/cm$^2$ produces a ponderomotive potential of 0.03 eV which is becoming comparable to the electron kinetic energy. However, the experimental evidence at 1.06-$\mu$m, which has a higher order of nonlinearity than at 532 nm,

still shows that doubly excited states are playing a role in the multiphoton process. Even though neither excitation scheme results in any detectable amounts of direct ionization, it also does not exclude the possibility that direct ionization could occur under the appropriate circumstances.

### B. Intensity effects

At low intensity, minimum-order perturbation theory predicts that for an $N$-photon process the number of counts should increase as $I^N$. This rapid intensity dependence of the signal for 0.532- and 1.06-$\mu$m excitation is illustrated in the log-log plots of Figs. 6(a) and 6(b), respectively. The points in Fig. 6(a) are measured by integrating the area under the electron peak for the singly ionized 0.88-eV channel [path (1)] and the doubly ionized 2.11-eV channel [path (3)]. These results were also separately verified by monitoring the total ion signal with a mass spectrometer as a function of intensity at 532 nm. Analysis of the linear portion of the log-log plot for the 0.88-eV channels gives a slope of $2.9\pm0.2$ and a saturation intensity, $I_S$, of $5\times10^{10}$ W/cm$^2$. This result is consistent with the 3-photon ionization of calcium. The dependence beyond the $I_S$ value is a consequence of the expanding focal volume[26] as the intensity is increased. Similarly, the 2.11-eV channel yields a slope of $6.2\pm0.4$ and $I_S=1.2\times10^{12}$ W/cm$^2$, which is in agreement with perturbative scaling laws.

The intensity dependence of the total ion yield for the two charge states for 1.06-$\mu$m excitation is shown in Fig. 6(b). Due to the degeneracy of the electron energies for paths (2) and (4) as discussed above, only the 6-photon process could be verified by monitoring the 0.88-eV channel at $I<1.1\times10^{11}$ W/cm$^2$. At these low intensities the ambiguity is removed from the electron spectrum since there is no appreciable yield of the $Ca^{2+}$ ion. The analysis of the total $Ca^+$-ion yield and the 0.88-eV electron channel gives a slope of $5.7\pm0.4$ and $I_S=7\times10^{10}$ W/cm$^2$. While analysis of the total $Ca^{2+}$-ion signal yields a slope of $10\pm1.5$ and an $I_S=2\times10^{11}$ W/cm$^2$. The slopes here are in good agreement with lowest order perturbation theory and a model consistent with sequential ionization.

Assuming that known scaling laws[27] are valid, the results reported here are in disagreement with the earlier work of Agostini and Petite[17] on the multiphoton ionization of calcium. Their experiment differs in that the pulse duration of their laser was 50 psec, as opposed to the 10-nsec pulses used in this study. Assuming that the saturation intensity is defined as the point at which the atomic population has been reduced to $e^{-1}$ of its initial value, one obtains a simple expression for the $N$th photon process:[27]

$$I_S=\sigma^{-1/N}\tau^{-1/N}, \tag{15}$$

where $\sigma$ is the generalized absorption cross section in units of cm$^{2N}$sec$^{N-1}$ and $\tau$ is the pulse duration. Obviously, $I_S$ increases with decreasing pulse duration and becomes less sensitive to changes in $\sigma$ and $\tau$ as the order of nonlinearity becomes large. Using this model to compare the results from excitation with a 10-nsec and 50-psec pulse gives a ratio of $I_S(50\text{ psec})/I_S(10\text{ nsec})$ equal to 2.4 and 1.6 for a 6- and 11-photon process, respectively. Table I gives the saturation intensity of this work and those estimated from Ref. 17 and the ratio of the two results. The measured ratio for the 6-photon ionization of calcium is approximately equal to 10, which differs from the factor of 2.4 predicted by Eq. (15). Likewise the 11-photon ionization of $Ca^+$ ion gives an experimental ratio of 4.5 as compared to 1.6 as given by Eq. (15). The uncertainty reported in both experiments are not sufficient to explain the differences with theory but are noted in this paper as a point of further study.

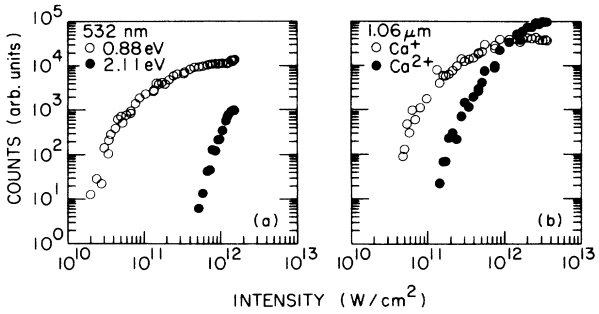


FIG. 6. Log-log plots of signal vs laser intensity for (a) 532-nm and (b) 1.06-$\mu$m radiation. See text and Table I for details.

### C. Angular distributions

Studies on electron angular distributions for multiphoton ionization provide valuable insight into the nature of the atomic transition and useful measurements for comparison to theory. However, as pointed out by Bucksbaum *et al.*,[1,25] at these intensities care must be taken in interpreting the origin of the observed angular distributions as purely atomic in nature. The scattering of the atomic electron distributions by the ponderomotive potential can severely alter the detected distribution.

TABLE I. Order of nonlinearity and saturation intensities for calcium.

| | 532 nm | | 1.06 $\mu$m | | Ref. 17 | $I_S/I_S^*$, 532 nm | |
|---|---|---|---|---|---|---|---|
| | $N$ | $I_S$ (W/cm$^2$) | $N$ | $I_S$ (W/cm$^2$) | $I_S^*$ (W/cm$^2$) | Expt. | Eq. (15) |
| $Ca^+$ | $2.9\pm0.2$ | $5.0\times10^{10}$ | $5.7\pm0.4$ | $7\times10^{10}$ | $(8-9)\times10^{11}$ | 10 | 2.4 |
| $Ca^{2+}$ | $6.2\pm0.4$ | $1.2\times10^{12}$ | $10\pm1.5$ | $2\times10^{11}$ | $(1-0.9)\times10^{12}$ | 4.5 | 1.6 |

This especially is true for low-energy electrons and at long wavelengths since the ponderomotive potential is proportional to $\omega^{-2}$. Similar scattering effects can be caused by appreciable space charge distributions. For our experiments the angular distributions were carefully evaluated to minimize any such effects and should be only representative of the multiphoton transition.

The electron angular distributions for the singly ionized 0.88-eV channel resulting from 532-nm and 1.06-$\mu$m excitation are shown in Fig. 7, as well as the 2.11-eV doubly ionized channel with 532-nm excitation. Due to the degeneracy in energy of the different electron channels at high intensity for 1.06-$\mu$m radiation, it was impossible to derive a meaningful result for any angular distributions except the 0.88-eV channel at low intensity. All the angular distribution studies were performed using linearly polarized light. The electron distributions were recorded by detecting electrons normal to the laser propagation direction and by rotating the polarization with respect to the detector axis. The azimuthal angle $\theta$ was varied over $2\pi$ to facilitate the detection of any asymmetries caused by imperfect alignment or optics. The points in Fig. 7 are the normalized results of the experiments. The most apparent difference in the shape of the distributions exists between the 0.88-eV channel at 532-nm and both the 0.88-eV channel at 1.06-$\mu$m or 2.11-eV channel at 532 nm. The last two processes are the result of a 6-photon absorption while the first is a 3-photon absorption. Consequently, the two 6-photon processes, Figs. 7(b) and 7(c), result in angular distributions which are highly peaked along the polarization direction as compared to the 3-photon process. This is indicative of the effects produced by solely increasing the order of nonlinearity in a *"single"-electron excitation.* In fact, the differences are directly comparable between the two 0.88-eV channel distributions at the two different wavelengths. Even comparison of the 2.11- and 0.88-eV channels seems reasonable considering that both processes originate from $S$ states.

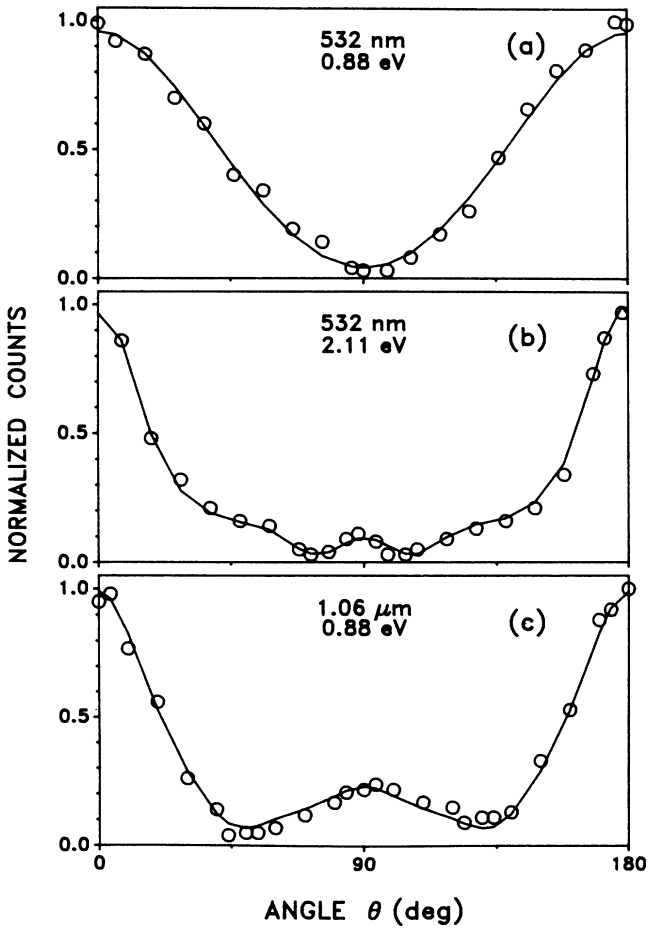


FIG. 7. Electron angular distributions for calcium. The open circles are the experimental data points and the solid lines are the results of the fit to Eq. (16). The three plots are (a) 532-nm excitation, 0.88-eV channel, (b) 532-nm excitation, 2.11-eV channel, and (c) 1.06-$\mu$m excitation, 0.88-eV channel. See text and Table II for details.

In order to extract some information about the radial elements involved in these multiphoton angular distributions the experimental data was fitted using a well-known expression derivable from lowest-order perturbation theory. Theoretically[22,28] it can be shown that a nonresonant $N$-photon process results in angular distributions of the form,

$$I(\theta) \propto \sum_{i=1}^{N} \beta_{2i} P_{2i}(\cos\theta) , \tag{16}$$

where $P_{2i}(\cos\theta)$ is the Legendre polynomial of order $2i$ and $\beta_{2i}$ are the atomic parameters which contain the information on the radial matrix elements. The experimental angular distributions were fit using Eq. (16) and the result of the fits are illustrated as solid lines in Fig. 7. Table II gives the $\beta_{2i}$ parameters and their standard deviation for each of the three distributions. The parameters are normalized with respect to $\beta_2$ and allowed to fit with the maximum number of $(N+1)$ terms. In order to test the goodness of the fits, analyses were conducted that included extra higher-order parameters in the expression; this resulted in no significant improvement in the fits.

Although the $\beta_{2i}$ atomic parameters derived from these fits are not very appealing physically and certainly would benefit from a comparison with theory, some qualitative observations can be made. As described above, as the order of the nonlinearity increases for a nonresonant

TABLE II. Atomic parameters from nonlinear least-squares fit to Eq. (16). Standard deviations are indicated in parentheses.

| | 0.88-eV channel | | 2.11-eV channel |
|---|---|---|---|
| | 532 nm | 1.06 $\mu$m | 532 nm |
| $\beta_0$ | 0.57(2) | 1.05(9) | 0.56(5) |
| $\beta_2$ | 1.00(3) | 1.00(10) | 1.00(9) |
| $\beta_4$ | 0.06(3) | 2.03(19) | 0.62(9) |
| $\beta_6$ | 0.11(4) | 0.53(14) | 0.44(11) |
| $\beta_8$ | | 0.24(14) | 0.49(11) |
| $\beta_{10}$ | | −0.03(15) | 0.00(11) |
| $\beta_{12}$ | | 0.14(14) | 0.17(12) |

process the higher-order parameters contribute to the fit resulting in a distribution that is more highly peaked along the laser polarization. This can be seen in Table II where the 6-photon processes have a significant contribution from the $\beta_8$ parameter. However, as the order of nonlinearity increases the trend in the fits seems to place less emphasis on the contributions from the highest allowable parameters. This is seen in the two, 6-photon fits in Table II where both highest-order parameters, $\beta_{10}$ and $\beta_{12}$, are nearly zero within their statistical certainty. This same trend in fits to Eq. (16) has been observed by other groups[29,30] studying nonresonant multiphoton ionization of rare-gas atoms. A simple quantum-mechanical argument would suggest that the transition matrix elements for final states with the highest orbital angular momentum are zero. Specifically for our experiments final states with $L=6$ do not contribute to the transition strength for the 6-photon process. One possible factor that could contribute to this effect extends the arguments used in Ref. 1 concerning the centrifugal barrier. However, for our situation the arguments must be modified to consider the effects of the effective potential at a *constant* electron energy. For linear polarized excitation the effect of the centrifugal barrier for a constant electron-energy channel can result in a suppression of high angular momentum states as the nonlinearity of the process increases. Our preliminary calculations seem to support this explanation but further study of this problem will be necessary.

## V. CONCLUSIONS

Single and double nonresonant ionization of calcium has been studied and the electron-energy spectrum analyzed at intensities less than $10^{13}$ W/cm$^2$. The main conclusions of this work are as follows.

(1) The role of electron correlations is observed to be significant for the nonlinear production of singly ionized calcium for both 0.532- and 1.06-$\mu$m radiation. Thus, the independent electron model would give an inadequate description of the ionization dynamics and a more complete model must incorporate correlation effects.

(2) The results exemplify the importance of the atomic structure in determining the overall ionization dynamics. The differences in atomic structure can ultimately determine which mechanism will dominate the ionization process.

(3) Sequential ionization is observed to be the dominant process responsible for the production of doubly ionized calcium. However, since electron correlations are observed to play an important role in the initial stages of ionization, it is conceivable that direct two electron ionization could occur under the proper choice of laser parameters. One such experiment is to tune a high intensity dye laser into near resonance with a known doubly excited state. This may enhance the amount of doubly excited character in the excitation process and could lead to appreciable branching into direct ionization.

A number of improvements to our system are currently in progress. These include the extension of our current studies by 3 orders in magnitude in laser intensity ($\simeq 10^{16}$ W/cm$^2$), reduction of our pulse duration to a few picoseconds, and improvements in the vacuum system.

## ACKNOWLEDGMENTS

The authors would like to thank C. H. Greene, P. Lambropoulos, and A. P. R. Rau for useful discussions. We would also like to acknowledge the technical advice of M. Bashkansky and T. F. Gallagher. This research was supported by the National Science Foundation under Grant No. PHY 86-03030. The research carried out at Brookhaven National Laboratory was supported by the U.S. Department of Energy.

[1]P. Bucksbaum, M. Bashkansky, R. R. Freeman, T. J. McIlrath, and L. F. DiMauro, Phys. Rev. Lett. **56**, 2590 (1986).

[2]P. Agostini, M. Clement, F. Fabre, and G. Petite, J. Phys. B **14**, L491 (1981).

[3]P. Kruit, J. Kimman, H. Muller, and M. Van der Wiel, Phys. Rev. A **28**, 248 (1983).

[4]K. Boyer, H. Egger, T. S. Luk, H. Pummer, and C. K. Rhodes, J. Opt. Soc. Am. B **1**, 4 (1984).

[5]T. S. Luk, H. Pummer, K. Boyer, M. Shakidi, H. Egger, and C. K. Rhodes, Phys. Rev. Lett. **51**, 110 (1983).

[6]A. L'Huillier, L. A. Lompre, G. Mainfray, and C. Manus, Phys. Rev. A **27**, 2503 (1983), Phys. Rev. Lett. **48**, 1814 (1982).

[7]I. S. Aleksakhin, N. B. Delone, I. P. Zapesochyi, and V. V. Suran, Zh. Eksp. Teor. Fiz. **76**, 887 (1979) [Sov. Phys.—JETP **49**, 447 (1979)].

[8]D. Feldmann and K. Welge, J. Phys. B **15**, 1651 (1982).

[9]See *Multiphoton Ionization of Atoms,* edited by S. L. Chin and P. Lambropoulos (Academic, Toronto, 1984).

[10]P. Lambropoulos, Phys. Rev. Lett. **58**, 108 (1987).

[11]K. Boyer and C. K. Rhodes, Phys. Rev. Lett. **54**, 1490 (1985); A. Szöke and C. K. Rhodes, *ibid.* **56**, 720 (1986).

[12]M. H. Mittleman, J. Phys. B **17**, L351 (1984); Phys. Rev. A **29**, 2245 (1984).

[13]A. Szöke, J. Phys. B **18**, L427 (1985).

[14]Z. Deng and J. Eberly, J. Phys. B **18**, L287 (1985).

[15]A. R. Reiss, Phys. Rev. A **22**, 1786 (1980); J. Phys. B **20**, L79 (1987).

[16]D. Feldmann, J. Krautwald, S. L. Chin, A. von Hellfeld, and K. H. Welge, J. Phys. B **15**, 1663 (1982).

[17]G. Petite and P. Agostini, J. Phys. (Paris) **47**, 795 (1986); P. Agostini and G. Petite, J. Phys. B **17**, L811 (1984).

[18]U. Eichmann, Y. Zhu, and T. F. Gallagher, J. Phys. B **20**, 4461 (1987).

[19]C. H. Greene and Longhaun Kim, Phys. Rev. A **36**, 45 (1987).

[20]Longhaun Kim and C. H. Greene, Phys. Rev. A **36**, 4272 (1987).

[21]G. Leuchs and H. Walther, in *Multiphoton Ionization of Atoms,* edited by S. L. Chin and P. Lambropoulos (Academic, Toronto, 1984), p. 109.

[22]P. Lambropoulos, Adv. At. Mol. Phys. **12**, 87 (1976).
[23]A. R. P. Rau, J. Opt. Soc. Am. B **4**, 784 (1987).
[24]K. Codling, L. J. Frasinski, P. Hatherly, and J. R. M. Barr, J. Phys. B **20**, L525 (1987).
[25]T. J. McIlrath, P. H. Bucksbaum, R. R. Freeman, and M. Bashkansky, Phys. Rev. A **35**, 4611 (1987).
[26]L. A. Lompre, A. L'Huillier, G. Mainfray, and C. Manus, Phys. Lett. **112A**, 319 (1985).
[27]P. Lambropoulos and X. Tang, J. Opt. Soc. Am. B **4**, 821 (1987).
[28]S. N. Dixit, J. Phys. B **16**, 1205 (1983).
[29]R. Hippler, H. J. Humpert, H. Schwier, S. Jetzke, and H. O. Lutz, J. Phys. B **16**, L713 (1983).
[30]F. Fabre, P. Agostini, G. Petite, and M. Clement, J. Phys. B **14**, L677 (1981).